Volatile Loss and Classification of Kuiper Belt Objects

R. E. Johnson – University of Virginia and New York University
A. Oza – University of Virginia and Université Pierre et Marie Curie
L. A. Young – Southwest Research Institute, Boulder
A. N. Volkov – University of Alabama
C. Schmidt – University of Virginia

Citation of published version:

Johnson, R. et al. (2015): Volatile Loss and Classification of Kuiper Belt Objects. *The Astrophysical Journal*, 809(1). DOI: 10.1088/0004-637X/809/1/43

The Astrophysical Journal, 809:43 (9pp), 2015 August 10 doi:10.1088/0004-637X/809/1/43

VOLATILE LOSS AND CLASSIFICATION OF KUIPER BELT OBJECTS

R. E. Johnson[1,2], A. Oza[3,4], L. A. Young[5], A. N. Volkov[6], and C. Schmidt[1,3]
[1] Engineering Physics, University of Virginia, Charlottesville, VA 22904, USA
[2] Physics, New York University, New York, NY 10003, USA
[3] Department of Astronomy, University of Virginia, Charlottesville, VA 22904, USA
[4] CNRS, LATMOS/IPSL, Université Pierre et Marie Curie, Paris, France
[5] SwRI, 1050 Walnut Street, Boulder, CO 80302-5150, USA
[6] Department of Mechanical Engineering, University of Alabama, Tuscaloosa, AL 35487, USA
Received 2015 March 14; accepted 2015 June 24; published 2015 August 7

ABSTRACT

Observations indicate that some of the largest Kuiper Belt Objects (KBOs) have retained volatiles in the gas phase (e.g., Pluto), while others have surface volatiles that might support a seasonal atmosphere (e.g., Eris). Since the presence of an atmosphere can affect their reflectance spectra and thermal balance, Schaller & Brown examined the role of volatile escape driven by solar heating of the surface. Guided by recent simulations, we estimate the loss of primordial N_2 for several large KBOs, accounting for escape driven by UV/EUV heating of the upper atmosphere as well as by solar heating of the surface. For the latter we present new simulations and for the former we scale recent detailed simulations of escape from Pluto using the energy limited escape model validated recently by molecular kinetic simulations. Unlike what has been assumed to date, we show that unless the N_2 atmosphere is thin ($<\sim 10^{18}$ N_2 cm^{-2}) and/or the radius small ($<\sim$200–300 km), escape is primarily driven by the UV/EUV radiation absorbed in the upper atmosphere. This affects the discussion of the relationship between atmospheric loss and the observed surface properties for a number of the KBOs examined. Our long-term goal is to connect detailed atmospheric loss simulations with a model for volatile transport for individual KBOs.

Key words: Kuiper belt objects: individual – planets and satellites: atmospheres

1. INTRODUCTION

Pluto's atmosphere was discovered through stellar occultation about a quarter of a century ago (e.g., Elliot et al. 1989), and the *Voyager* spacecraft measured Triton's atmosphere (Yelle et al. 1995). Now a number of large icy objects, at or past the orbit of Neptune, appear to have surface volatiles suggesting that vapor-pressure supported atmospheres are likely present during all or part of their orbits. We call these the volatile-bearing Kuiper Belt Objects (KBOs), although one is a moon of Neptune, and three (Pluto, Eris, and Makemake) are dwarf planets. KBOs are known to exhibit a variety of surfaces. How much of this variety is due to different origins and processing, and how much is due to common processes is uncertain. Schaller & Brown (2007) pointed out that the vapor-pressure supported atmosphere might provide a link. It controls the loss of the volatiles by escape, the appearance of radiation-induced chemical products on the surface, and the freshening of the surface through condensation. Here we improve upon the estimates of the loss of the primordial volatiles described in Schaller & Brown (2007 hereafter, SB) and also in Levi & Podolak (2009 hereafter, LP). This study is possible because of the growth in our knowledge of these bodies (e.g., Brown 2012) and recent molecular kinetic simulations of escape that re-examined both Jeans and hydrodynamic models for atmospheric escape (Volkov et al. 2011a, 2011b; Tucker et al. 2012; Erwin et al. 2013; Johnson et al. 2013b; Volkov 2015).

In this work we focus on loss of N_2, the most volatile species of the three (N_2, CH_4, CO) known to be present on Pluto and Triton and examined in SB and LP. These volatiles cannot be treated separately as a small amount of CO can be an important cooling agent and even a few percent of CH_4 dominates the heating of the upper atmosphere (Krasnopolsky & Cruikshank 1999). Therefore, we estimate the loss of the initial inventory of the most volatile species, N_2, from a number of KBOs having various sizes and orbital parameters. In these estimates we assume that trace amounts of the other species are present when the atmosphere is predominantly N_2. We first review the data on the KBOs of interest, then describe and critique the previous estimates for atmospheric escape and present improved approximate descriptions based on recent molecular kinetic and fluid simulations. Finally, new estimates for the retention of N_2 are presented and reviewed in light of the available observations.

2. PROPERTIES OF LARGE KBOS

We consider the eight largest bodies in the Kuiper Belt, including Neptune's moon, Triton, and Pluto's moon Charon. We exclude Haumea, since it is likely that the volatile retention is influenced more by collisions than by escape (Brown et al. 2007b). Table 1 lists the relevant properties: the radius of the body (r_0), its bulk density (ρ), and Bond albedo (A, more relevant than the geometric albedo for thermal balance); observations of their surfaces and atmospheres; and the semimajor axis (a) and eccentricity (e) of their orbits. For a number of these bodies, even Pluto, the densities and radii are not known accurately. For three KBOs we list a range of densities, and for Pluto, for which the mass is well constrained but not the radius, we list the parameters used in our recent simulations for consistency.

It is seen that these KBOs fall into classes in terms of size, albedo, heliocentric distances, and volatiles detected. Using improved estimates of the atmospheric loss rate we determine the net loss of N_2 from the larger, brighter bodies (Triton, Pluto, Eris, Makemake), which have retained a large fraction of their initial volatile inventory. We also re-evaluate the medium-sized bodies, 2007 OR10 and Quaoar, which have been

Table 1
KBO Properties Ordered by Radius

KBO[a]	a (AU)	e	r_0 (km)	ρ (g cm^{-3})	A A	Surface Composition	Atmosphere	References
Triton	30.04	0.01	1353	2.06	0.80[b]	N_2, CO, CH_4, H_2O, CO_2, C_2H_6; Heterogeneous.	~14 μbar, global @ 30 AU. N_2, trace CH_4, CO. Albedo suggests atmospheric freshening	Thomas (2000), McKinnon et al. (1995, p. 807) Stansberry et al. (1990), Grundy et al. (2010), DeMeo et al. (2010); Lellouch et al. (2010)
Pluto	39.17	0.24	1178	1.91	0.67[c]	N_2, CO, CH_4, tholins, C_2H_6, little/no H_2O; Heterogeneous.	~17 μbar, global @ 30–32 AU, N_2 trace CH_4, CO. Albedo suggests atmospheric freshening	Lellouch et al. (2009, 2011), Buie et al. (2006), Grundy et al. (2014), Holler et al. (2014)
Eris	67.94	0.43	1163	2.52	0.55	N_2, CH_4	<1 nbar @ 96 AU. Albedo suggests atmospheric freshening.	Sicardy et al. (2011); Tegler et al. (2012), Abernathy et al. (2009)
Makemake	45.57	0.16	733	1.6–2.1[d]	0.62	N_2, CH_4, C_2H_6 Heterogeneous.	<12 nbar @ 52 AU. Albedo suggests atmospheric freshening.	Ortiz et al. (2012); Lim et al. (2010), Stansberry et al. (2008, p. 161) Tegler et al. (2008), Brown et al. 2007a
2007 OR_{10}	66.88	0.50	640	1.6–2.1[d]	0.06	CH_4 (inferred); H_2O	No constraints @85–87 AU.	Santos-Sanz et al. (2012), Brown et al. (2011)
Charon	39.17	0.24	606	1.72	0.25	H_2O, NH_3	<110 nbar N_2 and <15 nbar CH_4 @ 31 AU.	Person et al. (2006); Brozović et al. 2015, Lellouch et al. (2011), Cook et al. (2007), Gulbis et al. (2006)
Quaoar	43.18	0.04	534	2.18	0.07	N_2 (v. tentative), CH_4, H_2O, C_2H_6, "dark material"	<20 nbar CH_4 @ 43 AU.	Fornasier et al. (2013), Dalle Ore et al. (2009), Schaller & Brown (2007), Braga-Ribas et al. (2013)
Sedna	541.79	0.86	498	1.6–2.1[d]	0.19	H_2O, serpentine, N_2 (trace), CH_4 (trace), C_2H_6 (trace), tholins.	Occultation, with no atmospheric analysis @ 87 AU.	Pál et al. (2012). Emery et al. (2007), Barucci et al. (2010), Braga-Ribas (2013)

Notes.
[a] a, semimajor axis; e, orbital eccentricity; r_0, average surface radius; ρ, mass density; A, bond albedo.
[b] South polar cap.
[c] N_2-rich terrain.
[d] No known satellite, density assumed Charon-like to Pluto/Triton-like.

suggested to have lost most or all of their initial N_2 component (SB), with their low albedos, likely a result of radiation processing of gaseous or condensed methane (e.g., Johnson 1989; Strazzulla et al. 2003). Charon and Sedna are outliers with intermediate albedos, the former having rapidly lost its primordial volatiles but continuously acquires nitrogen from Pluto (Tucker et al. 2015), and the latter in a very distant orbit with a very thin atmosphere having retained its volatiles. Data from Table 1, modified as discussed in the text, is used below to calculate atmospheric loss rates for KBOs in their current orbits. The role of the evolution of the orbits and albedos will be considered in the future.

3. ATMOSPHERIC ESCAPE MODELS

Escape can be driven by heating of the surface by the solar visible radiation and by direct absorption solar radiation in the atmosphere. We first discuss escape of volatiles from KBOs driven by surface heating as in SB and LP. We then discuss the escape driven by heating of the upper atmosphere. We only consider a nitrogen-dominated atmosphere, the most volatile of the three species considered. The applicability of the various escape processes depends on how tightly bound and rarefied the atmosphere is, qualities indicated by the surface values of the Jeans parameter, λ_0, and an atmospheric column density, N_0.

The Jeans parameter is the ratio of potential energy, $U = GM_{\rm KBO}\, m/r$, to thermal energy, kT, which at the surface, $r = r_0$, is written as $\lambda_0 = U_0/(kT_0)$. Here $U(r)$ is the gravitational binding energy for a molecule of mass m to a KBO of mass $M_{\rm KBO}$, G is the gravitational constant, and k is the Boltzmann constant. Following SB we assume an average surface temperature, T_0, in radiative equilibrium: $\varepsilon\sigma T_0^4 = [F_{\rm 1AU}(1\text{-}A)/R^2]/4$, where ε is the emissivity, $F_{\rm 1AU}$ is the solar insolation at 1 AU, A is the bolometric Bond albedo, R is the orbital position in AU, σ the Stefan–Boltzmann constant and the factor of four accounts for global averaging. The surface temperature is, of course, influenced by thermal inertia and latent heat of sublimation (Young & McKinnon 2013), which will be addressed in later work.

The Jeans parameter is also related to the atmospheric scale height at the surface, H_0, by $H_0 = r_0/\lambda_0$, with a large λ_0 indicating a tightly bound atmosphere. We use a column density $N_0 = n_0 H_0$ as a parameter, where n_0 is the number density at the surface so that $N_0 = P_{\rm vap}(T_0)/(mg_0)$: using $P_0 = n_0\, kT_0$, $P_0 = P_{\rm vap}(T_0)$, $g_0 = GM_{\rm KBO}/r_0^2$ the surface gravity, and $P_{\rm vap}$ the vapor pressure of the N_2 surface frost. In Figure 1 we show the range of λ_0 and N_0 of interest. We use N_0 rather than P_0 to characterize the KBO atmospheres, as it is also related to the zenith column (Elliot & Young 1992) which determines the transition between escape processes discussed in Section 3. It is seen in Figure 1 that the KBOs of interest have moderately bound atmospheres, with λ_0 in the range of 10–100. λ_0 varies inversely with the temperature, which itself slowly varies as $R^{-1/2}$ over an orbit. Sedna, with aphelion at ~1000 AU, reaches $\lambda_0 \sim 60$ at a very small N_0, still only a factor of 4 larger than its perihelion value. In contrast, because the surface pressure depends very strongly on the temperature of the N_2 ice, N_0 can vary dramatically over a KBO's season.

Accurately modeling escape from an atmosphere of a KBO heated at the surface by the solar radiation and with the upper atmosphere heated in the UV/EUV requires detailed knowledge of the altitude dependence of the composition, chemistry and volatile transport (e.g., Young 2012; Zhu et al. 2014). Therefore, consistent with our present understanding of the KBOs, simpler models are still warranted. We first critique the estimates for escape driven by surface heating using recent fluid and molecular kinetic simulations. This is followed by a description of a model that estimates escape due to short wavelength heating of the upper atmosphere. We then combine the surface and atmospheric heating in order to estimate the net loss rates.

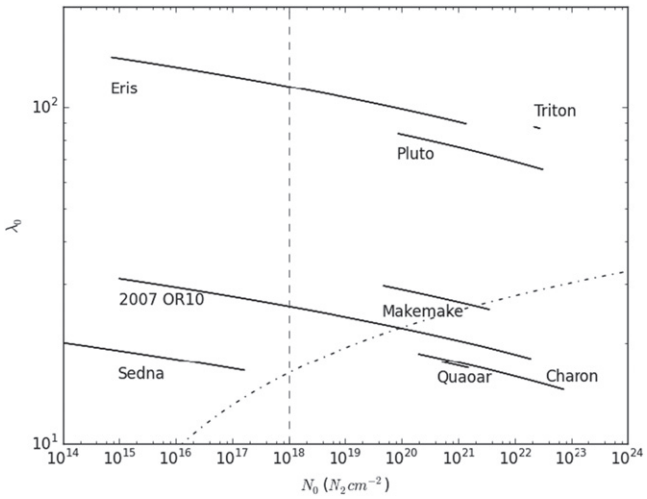

Figure 1. Range of Jeans parameter at the surface, λ_0, vs. column density, N_0, for an N_2 atmosphere on a number of KBOs over their orbit around the Sun using the data in Table 1 for a, e, r_0, and ρ *but* using $\varepsilon = 0.8$ and $A = 0.67$, appropriate for an early KBO with a bright, N_2-covered surface as discussed in the text. For Makemake, 2007OR10, and Sedna with uncertain densities in Table 1 we used $\rho = 1.8\ {\rm g\ cm^{-3}}$. Sedna's values shown are only near perihelion as its aphelion ($N_0 << 10^{14}$ cm^{-2}) is off-scale. Dashed line: $N_0 = N_c = 10^{18}$ N_2 cm^{-2}; to the right the CH_4 component is sufficient to absorb the UV (discussed in Section 3.2). Dotted–dashed line: (calculated loss rate/SJ loss rate) = 1 from Figures 2(a) and (b); Equation (1*b*) used in SB *overestimates* the surface-heating-induced escape rate below and *underestimates* it above this line.

3.1. Escape Driven by Surface Heating

Rates for atmospheric loss driven *only* by the solar heating of the surface have been applied to KBOs in both SB and LP. The latter used Parker's isentropic fluid model of escape from KBOs determined by the surface temperature in which the thermal conduction is neglected. However, for an N_2 atmosphere driven *only* by surface heating, molecular kinetic simulations have shown that such results only apply for λ_0 much smaller than those in Figure 1 (e.g., Volkov et al. 2011a; Volkov & Johnson 2013; Volkov 2015).

Estimates of the atmospheric loss rate using the Jeans formula evaluated at the surface, rather than at the exobase, were suggested to be lower bounds in SB. In this way they avoid determining the exobase properties and they could also calculate the loss rates for three species (N_2, CH_4, CO) separately. For a body of radius, r_0, having a uniform surface temperature, T_0, the surface *sublimation rate* for molecules with mass m and vapor pressure $P_{\rm vap}$ is given by

$$(dM/dt)_0 = 4\pi r_0^2 m\left[P_{\rm vap}(T_0)/(2\pi mkT_0)^{0.5}\right] \qquad (1a)$$

multiplied by the fractional coverage of the surface by the volatile. For an atmosphere for which escape can occur directly

from the surface, one writes the loss rate as

$$(dM/dt)_{\rm SJ} = (dM/dt)_0(1 + \lambda_0)\exp(-\lambda_0). \quad (1b)$$

In the following we will call Equation (1*b*) the surface-Jeans (SJ) approximation. In SB it was suggested that if heating of the upper atmosphere is ignored, this rate is a lower bound to the actual escape rate. For a hydrostatic, isothermal atmosphere with no UV absorption in the upper atmosphere, this is correct as the ratio of the Jeans rate at the exobase to the SJ rate is $\sim r_x/r_0$, where r_x is the exobase radius.

Atmospheres experiencing escape are, of course, *not isothermal*. Therefore, the estimate in Equation (1*b*) was tested earlier by simulations of escape driven only by the surface heating. In Volkov et al. (2011a, 2011b) a molecular kinetic model, the Direct Simulation Monte Carlo method, was used which correctly describes the transition from the collisional (fluid) regime to a collisionless escaping gas. It was shown (e.g., Figure 10(b) in Volkov et al. 2011b) that for a range of λ_0 and column densities the SJ rate can considerably over estimate the loss rate. Since such simulations are computationally expensive we also use the Fluid-Jeans (FJ) model which has been tested by molecular kinetic simulations for the larger λ_0 and N_0 in Figure 1. In this model, the one-dimensional equations for an inviscid, heat conducting gas are solved *iteratively* by applying the Jeans mass and energy escape rates at the upper boundary and taking into account the non-zero gas flow speed (Yelle 2004; Volkov et al. 2011a, 2011b). Instead of N_0, Volkov et al. (2011a, 2011b) used the surface value of radial Knudsen number, Kn_0, a common parameter in fluid dynamics. It is the ratio of the mean free path between collisions, $l_0 = 1/(n_0\sigma_{\rm eff})$, to a length scale, here r_0: $Kn_0 = 1/(n_0\sigma_{\rm eff}\, r_0)$, where $\sigma_{\rm eff}$ is an effective cross section for collisions between atmospheric molecules: Kn_0 and N_0 are related by $Kn_0 = 1/(\lambda_0\sigma_{\rm eff}\, N_0)$.

In Figure 2 we give escape rates driven only by surface heating from an N_2 atmosphere calculated using the FJ (solid curves in Figures 2(a) and (b)) and kinetic (dashed curves in Figure 2(b)) simulations. The dash–dot curves in Figure 2(a) are an analytic estimate to be discussed. The N_2 loss rates in Figure 2 are divided by the SJ rate in Equation (1*b*) used in SB. Because molecular kinetic simulations in Figure 2(b) are computationally intense, results are given only for $\lambda_0 = 10$ and 15 at the smaller N_0 of interest where the ratio initially increases with increasing N_0 for each λ_0 (Volkov et al. 2011b). These are compared to the FJ simulations performed assuming that the upper boundary coincides with the nominal exobase. It is seen in Figure 2(b) that the FJ results underestimate the loss rate the smaller N_0. Increasing the upper boundary can reduce the difference (e.g., Tucker & Johnson 2009; Volkov et al. 2011b). However, at the larger N_0 in Figure 2(b), the FJ simulations merge with the kinetic simulations and so can be used as a reasonable approximation to the loss rate at larger N_0 (Volkov et al. 2011a, 2011b). This is the conduction dominated regime, the so-called Fourier regime discussed in Gruzinov (2011), in which the ratio for fixed λ_0 in Figures 2(a) varies as $\sim 1/N_0$ at large N_0. That is, as N_0 increases, the exobase increases in altitude, the exobase density rapidly drops and temperature at the exobase also drops. For these reasons the number of the molecules that have energies greater than the escape energy drops rapidly as does the corresponding escape rate.

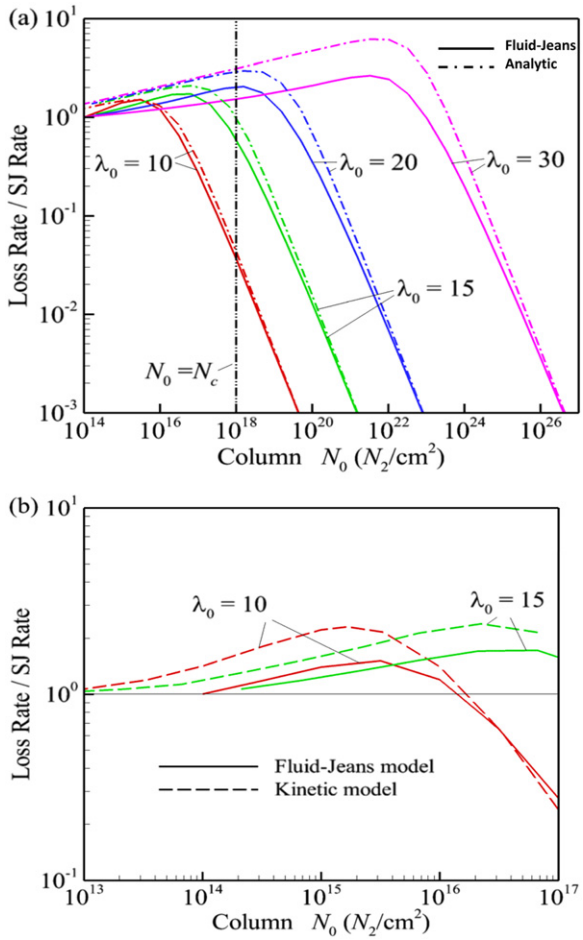

Figure 2. Loss rate from an N_2 atmosphere produced by surface heating scaled to the SJ rate in Equation (1*b*) for a number of λ_0 as a function of column density N_0 calculated with the FJ model (solid curves in 2(a) and (b)), and kinetic model (dashed curves in 2(b)). Also shown in 2(a): a rough fit (dashed–dotted curves) given in Equation (2*a*) as $R_{\rm fit}$; dashed–double-dotted line, $N_0 = N_c$ minimum atmosphere for absorption of UV as discussed. Results of kinetic simulations in 2(b) calculated as in Volkov et al. (2011a, 2011b); instead of N_0 they used $Kn_0 = 1/(n_0\sigma_{\rm eff}r_0) \sim 1/(\lambda_0\sigma_{\rm eff}N_0)$, where $\sigma_{\rm eff} = 2^{1/2}\sigma(T_0)$ with $\sigma(T_0)$ the collision cross section of pseudo-Maxwellian molecules at temperature T_0: although slowly dependent on T_0 an average value, $\sigma_{\rm eff} = 1.0 \times 10^{-14}$ cm^2 for $N_2 + N_2$ collisions was used.

In order to apply the results in Figure 2 to the KBOs of interest we use an analytic approximation to the ratio of the simulated escape rate to the SJ rate, $R_{\rm fit}$. We fit the kinetic simulations in Figure 2(b), which are accurate at small N_0, as $R_1 \sim (1/Kn_0)^{0.09}$ and the asymptotic behavior of the FJ model in Figure 2(a), which is accurate at large N_0, as $R_2 \sim 70\,[Kn_0\exp(\lambda_0)]/\lambda_0^{2.55}$. These are combined as

$$R_{\rm fit}^{-1} = R_1^{-1} + R_2^{-1} \quad (2a)$$

giving the dash–dot curve in Figure 2(a), which we will use in the remainder of the paper. In the absence of kinetic results at all N_0 and λ_0 of interest in Figure 1, the escape driven by heating of the surface, $(dM/dt)_S$, is estimated as

$$(dM/dt)_S \sim R_{\rm fit}\,(dM/dt)_{\rm SJ} \quad (2b)$$

using $R_{\rm fit}$ from Equation (2*a*) and $(dM/dt)_{\rm SJ}$ from Equation (1*b*).

Before discussing the atmospheric heating component, we note that the ratios in Figures 2(a) and (b) indicate that the SJ rate *is a lower bound* to the escape rate at small N_0 for each λ_0,

as suggested in SB, but can hugely *overestimate* the loss rate at large N_0. For instance, for a KBO with $\lambda_0 \sim 10$, the SJ estimate is a lower bound to the thermally driven rate for $N_0 < \sim 10^{16}$ $N_2\,cm^{-2}$. The change from the SJ rate from being a lower bound to being an upper bound moves to larger N_0 as λ_0 increases, indicated by the dot–dash line in Figure 1. Therefore, for Quaoar and Charon, as well as Makemake and 2007 OR10 near perihelion, the SJ rates significantly overestimate escape driven by surface heating. Below we describe an approximation for the UV/EUV driven escape which we will combine with the approximation in Equation (2*b*).

3.2. UV/EUV Driven Escape

Detailed simulations for escape from Pluto's atmosphere show that escape is dominated by heating of the upper atmosphere and not by the surface temperature. That is, near perihelion where $\lambda_0 \sim 60$, rather than losing $\sim 1.6 \times 10^{11}\,N_2\,s^{-1}$, as estimated using Equation (1*b*), Pluto loses ~ 2.6–$3.5 \times 10^{27}\,N_2\,s^{-1}$ at solar medium conditions due the upper atmospheric heating (Erwin et al. 2013). When the radiation absorbed in the upper atmosphere is important the volatiles cannot be treated separately. That is, UV absorption by the small concentration of CH_4 in Pluto's atmosphere dominates the upper atmospheric heating. This largely results from CH_4 photolysis by Lyα, a wavelength at which pure nitrogen atmospheres are transparent. If a KBO has retained a significant column of N_2, then the less volatile CH_4 will be present as a trace species, as is the case at Triton and Pluto. Therefore, we estimate the loss of the primordial nitrogen from an N_2 atmosphere having a small fraction of CH_4, which would be typical of early KBO atmospheres.

To simulate N_2 escape from Pluto in response to the solar heating, a description of the atmosphere as a function of altitude was required. Fortunately, it was also shown that the so-called energy limited (EL) loss rate gave a reasonable estimate of the globally averaged escape rate (Tucker et al. 2012; Erwin et al. 2013). This estimate is based on the assumption that the energy absorbed in the upper atmospheres can be removed more efficiently by escape than by downward thermal condition or radiation to space (e.g., Erwin et al. 2013; Figure 4). In its simplest form, the globally integrated escape rate is approximated as:

$$(dM/dt)_{\rm EL} \sim mQ(r_a)/U(r). \tag{3a}$$

Here m is the molecular mass, $Q(r_a)$ is the upper atmosphere heating rate, $U(r)$ is the average gravitational energy of the molecules at r, and r_a is a radius below the peak in the UV absorption, well below the exobase, r_x, and well above the physical surface, r_0. Because molecules lost to space must overcome gravity, in steady state, they are replaced from a radius r near or below r_a. Using $r \sim r_a$, the expression in Equation (3*a*) was shown to accurately approximate the results of molecular kinetic simulations for a range of upper atmospheric heating rates (Johnson et al. 2013b). It was also shown that this approximation is most accurate when the escape rate is large but Jeans-like rather than when the heated upper atmosphere goes sonic, opposite to what was assumed for years.

The heating rate is often written as

$$Q(r_a) = \eta 4\pi r_a^2 \langle F_{\rm EUV/UV} \rangle. \tag{3b}$$

Here $\langle F_{\rm EUV/UV} \rangle$ is the *globally averaged* energy flux absorbed in the UV and EUV, and η is the heating efficiency. Since heating expands the upper atmosphere, both r_a and r_x increase relative to r_0 as Q increases, enhancing the KBO's cross sectional area for absorption of radiation. The peak in the UV heating at Pluto occurrs at ~ 1.2–$1.3 r_P$, depending slowly on the solar conditions where r_P is Pluto's radius. Using such values for r and r_a in Equations (3*a*) and (3*b*) gave reasonable agreement with detailed simulations for both solar minimum and maximum conditions (Erwin et al. 2013: Table 4). Therefore, in scaling the UV/EUV heating and the escape from KBOs to the rates in Erwin et al. (2013), we are essentially assuming $r \sim r_a \sim 1.2$–$1.3 r_0$ in Equations (3*a*) and (3*b*).

Although more detailed expressions for the EL rate in Equation (3*a*) have been discussed (e.g., Lammer et al. 2009), we have shown that the accuracy depends primarily on the accuracy of the heating rate, Q, in Equation (3*b*). The effective cross section for absorption in the EUV by $N_2 \sim 0.91 \times 10^{-17}\,cm^2$ and that for absorption in the UV by CH_4 is $\sim 1.8 \times 10^{-17}\,cm^2$ (Krasnopolsky & Cruikshank 1999). To achieve an optical depth of ~ 1 in the UV requires a line of sight column of $\sim 5.5 \times 10^{16}\,CH_4\,cm^{-2}$. Although the mixing ratios are uncertain, by scaling the heating rate to that used in the simulations of Pluto's upper atmosphere (a CH_4 mixing ratio of $\sim 2\%$–3%) requires a minimum atmospheric column of $\sim 2 \times 10^{18}\,N_2\,cm^{-2}$ to achieve unit optical depth in the UV. The globally averaged heating rate is typically estimated using an average solar illumination angle of $\sim 60^{\rm o}$ (e.g., Strobel et al. 1996) in which case a radial column density $> \sim 1 \times 10^{18}\,N_2\,cm^{-2}$ is roughly required to obtain an average optical depth of unity in the UV. At these column densities, N_2 is also optically thick in the EUV, which contributes at $< \sim 20\%$ level to the total UV/EUV heating. Therefore, in applying the EL estimate of the UV/EUV-induced N_2 loss rate, we require that $N_0 > N_c = 10^{18}\,N_2\,cm^{-2}$.

Since the EL rate is linear in Q, we can estimate the loss of N_2 for each KBO by scaling to the simulations for Pluto which used heating rates from Krasnopolsky & Cruikshank (1999) and Krasnopolsky (1999). At 30 AU for solar medium conditions, their globally averaged CH_4 value for $\eta \langle F_{\rm EUV/UV} \rangle$ is $1.4 \times 10^{-3}\,ergs\,cm^{-2}\,s^{-1}$, which includes the Ly$\alpha$ resonantly scattered by the interplanetary medium, and their N_2 value for $\eta \langle F_{\rm EUV/UV} \rangle$ is $0.29 \times 10^{-3}\,erg\,cm^{-2}\,s^{-1}$. The N_2 rate due to direct sunlight shortward of 800 Å scales as R^{-2}, where R is the radial distance from the Sun in AU. Due to Lyα absorption and scattering, the radial dependence of the UV heating of CH_4 is more complicated. It consists of the direct solar flux, which is gradually attenuated, the scattered interplanetary Lyα (Gladstone 1998; Quémerais et al. 2013) and an integrated stellar source. Because we are considering globally averaged loss rates and average solar conditions, we assume the sum of the direct and scattered solar UV scale as $\sim R^{-2}$. To this we add a constant stellar Lyα background which eventually dominates at large R. Therefore, $\eta \langle F_{\rm EUV/UV} \rangle$ in Equation (3*b*) scales to that at Pluto as $\sim [(30/R)^2 + 0.09)]$. Substituting $Q(r_a)$ from Equation (3*b*) and the expression for

U into Equation (3*a*), and assuming r_a is proportional to r_0, the EL mass loss rate for N_2 can be scaled to that for escape from Pluto. Therefore, in order to calculate escape due to heating of the upper atmosphere, $(dM/dt)_U$, we will use:

$$(dM/dt)_U \sim (dM/dt)_{\rm EL} \sim (\rho_{\rm P}/\rho_{\rm KBO}) \times [(30/R)^2 + 0.09](dM/dt)_{\rm P}. \quad (4)$$

Here $\rho_{\rm P} = 2.05\,{\rm g\,cm^{-3}}$ and $(dM/dt)_{\rm P} = 120\,{\rm kg\,s^{-1}}$ are the density used and mass loss rate calculated for Pluto at 30 AU in Erwin et al. (2013). Below we combine the estimate for escape driven by heating of the surface in Equation (2*b*) with that for radiation absorption in the atmosphere in Equation (4).

3.3. Combined Surface and Upper Atmosphere Heating

Loss from KBO atmospheres can be driven by solar heating of the surface (or of a deep haze layer), as well as by the UV/EUV heating of the upper atmosphere. Zhu et al. (2014) combined the upper atmosphere model of Erwin et al. (2013) with a model of Pluto's lower atmosphere. They found a slightly larger (~30%) loss rate than in Erwin et al. (2013). Because escape due only to the surface temperature is negligible, synergy between surface heating of the lower atmosphere and the direct heating of the upper atmosphere might be occurring. Since that result is now being re-examined, the escape rates in Erwin et al. (2013) will be used here. We also note that the EL approximation to escape driven by upper atmospheric heating can overestimate the escape rate if the outward gas flow goes sonic or Q becomes very small. Based on the criterion in Johnson et al. (2013b), sonic escape due to atmospheric heating does not occur for the KBOs of interest and surface heating contributes when Q becomes small. Therefore, at each orbital position, R, we simply use the larger of loss due to surface heating, $(dM/dt)_{\rm S}$ from Equation (2*b*), and upper atmospheric heating, $(dM/dt)_{\rm U}$ from Equation (4), as a conservative estimate of the net escape rate from a KBO. The surface heating rate is very sensitive to the albedo, which can change over time, and both $(dM/dt)_{\rm S}$ and $(dM/dt)_{\rm U}$ depend on the mass density, which is not well constrained for a number of the KBOs in Table 1. Our estimate of $(dM/dt)_{\rm U}$ is also subject to the two constraints: the surface sublimation rate in Equation (1*a*) must exceed the escape rate, which is always be the case for the KBOs examined, and there must be a sufficient column of gas ($N_0 > N_c$) to account for the CH_4 contribution to the heating as indicated in Figure 1. To roughly indicate the uncertainties in our estimates of the total loss, we also use an ad hoc model in which the loss processes are added in the form, $(dM/dt) \sim (dM/dt)_{\rm S} + f_{\rm UV}\,(dM/dt)_{\rm U}$, using $f_{\rm UV} \sim [1 - \exp(-\alpha\, N_0/N_c)]$ where α is a parameter to be chosen. In this way $f_{\rm UV}$ acts to gradually cut-off the UV/EUV contribution as the atmosphere becomes thin: i.e., as $N_0 \rightarrow 0$, $f_{\rm UV} \rightarrow (-\alpha N_0/N_c)$ reducing the heating rate. After presenting the results below we conclude by discussing their relevance.

4. RESULTS

The shaded areas in Figure 3 indicate the range of radial distances, R, and KBO radial size, r_0, for which the estimate of the escape rate driven by UV/EUV absorption, $(dM/dt)_{\rm U}$ from Equation (4), dominates escape due to surface heating, $(dM/dt)_{\rm S}$ from Equation (2*b*). This is shown for two different bond albedos and an average mass density. The nearly vertical (red) solid and dashed curves ($A = 0.67$ and 0.1 respectively) indicate where $(dM/dt)_{\rm U} = (dM/dt)_{\rm S}$. The nearly horizontal (blue) solid and dashed curves indicate where $N_0 = N_c$ for each albedo. Therefore, the light-gray area is the region for which $(dM/dt)_{\rm U} > (dM/dt)_{\rm S}$ assuming $A = 0.67$. The extension of that region assuming much darker surfaces ($A = 0.1$), having higher surface temperatures and larger column densities, is indicated by the dark gray region. The primary effect of the lower albedo is that the atmosphere remains sufficiently thick to absorb the UV ($N_0 > N_c$) out to much larger distances from the Sun. For comparison, the radial size and orbital range for the KBOs in Table 1 are indicated by labeled vertical lines.

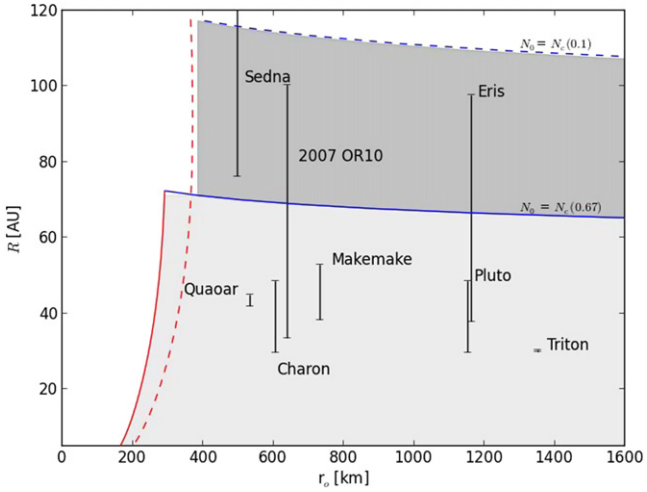

Figure 3. Comparison of $(dM/dt)_{\rm U}$ *and* $(dM/dt)_{\rm S}$ for KBOs having an early N_2 atmosphere vs. distance from Sun, R, vs. radius, r_0. $(dM/dt)_{\rm U}$ dominates in shaded regions. Solid curves: $(dM/dt)_{\rm S}$ and N_0 calculated for an N_2 atmosphere with a surface frost using $A = 0.67$: $\varepsilon = 0.8$. Dashed curves: $(dM/dt)_{\rm S}$ and N_0 calculated for T_0 obtained using $A = 0.1$: $\varepsilon = 0.8$. Nearly vertical (red) curves: $(dM/dt)_{\rm S} = (dM/dt)_{\rm U}$; nearly horizontal (blue): $N_0 = N_c = 10^{18} N_2\ {\rm cm^{-2}}$. The straight vertical lines indicate the orbital range of each the KBO in Table 1. Used an average density, $\rho_{\rm KBO} = 1.8\ {\rm g\,cm^{-3}}$, as in Figure 1 in SB.

It is seen in Figure 3 that, except for Sedna, the evolution of the nitrogen component of the atmospheres of the KBOs of interest can be dominated by escape driven by upper atmospheric heating. This is the case unless the body is small, $r_0 < \sim 300$ km, or the atmospheric column becomes too thin to fully absorb the UV ($N_0 < N_c$). If the surface has a relatively bright frost ($A = 0.67$: solid lines) the atmosphere is thin on Sedna over its full orbit, but only beyond ~70 AU for Eris and 2007OR10. During the time in which they retain significant N_2 and a relatively bright surface frost, the dominant mass loss process is seen to change with distance from the Sun. In Figure 4 we show this explicitly for 2007OR10 again using $\rho_{\rm KBO} = 1.8\ {\rm g\,cm^{-3}}$ and the two different albedos to calculate $(dM/dt)_{\rm S}$ and N_0. The solid and dot–dash lines are for $A = 0.67$ and 0.1 respectively using the larger of $(dM/dt)_{\rm S}$ and $(dM/dt)_{\rm U}$. For comparison, the dashed lines in Figure 4 is calculated assuming the upper atmospheric heating is reduced gradually as the atmosphere becomes thin: $(dM/dt) \sim (dM/dt)_{\rm S} + [1 - \exp(-\alpha N_0/N_c)](dM/dt)_{\rm U}$ with $\alpha = 0.1$ and $A = 0.67$. Consistent with Figure 3, $(dM/dt)_{\rm U}$ dominates not only at the smaller values of R, but also dominates the net loss rate.

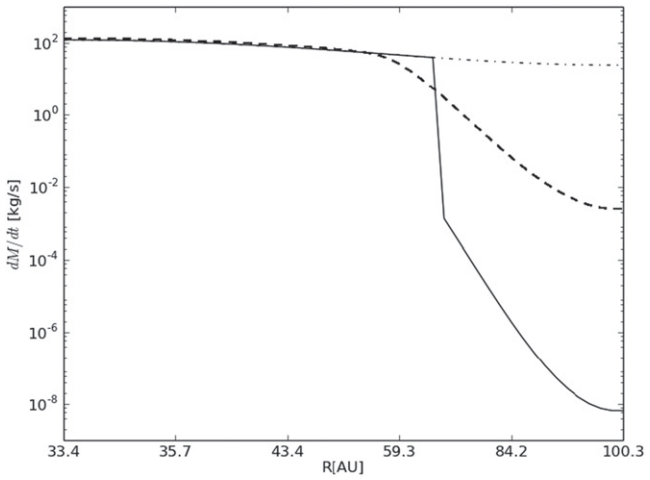

Figure 4. 2007OR10: mass loss rate, (dM/dt), for N_2 atmosphere containing a Pluto-like fraction of CH_4 vs. radial distance, R, from the Sun in AU using $\rho = 1.8$ g cm^{-3} as in Figure 3; (solid curve) using the larger of $(dM/dt)_U$ from Equation (4) and $(dM/dt)_S$ in Equation (2*b*) with $A = 0.67$: the mass loss rate averaged over an orbit in Equation (5) is $\langle dM/dt\rangle \sim 26$ kg s^{-1}; (dash–dot curve): same using $A = 0.1$ indicating a huge change in $(dM/dt)_S$ with the orbit average, $\langle dM/dt\rangle \sim 44$ kg s^{-1}; (dashed curve) $(dM/dt) = (dM/dt)_S + f_{UV}(dM/dt)_U$ with $f_{UV} = 1 - \exp(-\alpha N_0/N_c)$ and $\alpha = 0.1$: difference in $\langle dM/dt\rangle$ from solid line is a few percent.

Integrating over each KBO's orbit, the average mass loss rate, $\langle dM/dt\rangle$, is

$$\langle dM/dt\rangle = \int (dM/dt)dt/\tau_{KBO} = \int (dM/dt)\left(R^2/2\pi ab\right)d\theta. \quad (5)$$

That is, the time integral over the orbit is related to the integral over the true anomaly through *Kepler*'s second law ($R^2 d\theta/dt = 2\pi\, ab/\tau_{KBO}$) where a and b are the semimajor and minor axes of the orbit, θ the angular position in the orbit (i.e., the true anomaly), τ_{KBO} the orbital period and (dM/dt) the mass loss rate at each R. Although Eris and 2007OR10 have similar orbital ranges, the effect of the surface albedo for the much more massive Eris is a few percent, but that is not the case for 2007OR10 as seen from Figure 4. It is also seen that the effect of the gradual transition (dashed line) is only a few percent. However, the orbital-averaged N_2 loss rate, $\langle dM/dt\rangle$, increases from 26 kg s^{-1} for $A = 0.67$ (solid line) to 44 kg s^{-1} for $A = 0.1$ (dotted–dashed line). This large increase is primarily due to the larger radial region for which 2007OR10 surface temperature is such that it has sufficient column to absorb the UV out to large distances from the Sun, as indicated in Figure 3 by the dark shaded area.

In Table 2 we summarize orbital-averaged loss rates for the KBOs in Table 1. Estimates of escape driven *only* by surface heating are given in the SJ approximation used in SB, $\langle dM/dt\rangle_{SJ}$ using Equation (1*b*), and then improved upon, $\langle dM/dt\rangle_S$ using Equation (2*b*). For comparison, results are also shown for loss driven by upper atmosphere heating, $\langle dM/dt\rangle_U$ using Equation (4) and ignoring the thin-atmosphere cut-off. Orbital-averaged loss rates, $\langle dM/dt\rangle$, are then given using the dominant process at each R and accounting for the thin atmosphere cut-off, N_c. For each KBO we use the mass, radius and orbital properties from Table 1. The results in Table 2 are for N_2 escape *prior* to loss of the full primordial nitrogen inventory. Therefore, we assume a relatively bright surface with $A \sim 0.67$ as seen in Table 1 for Pluto. For Makemake, 2007OR10, and Sedna we use both the upper and lower estimates of the density. Not surprisingly, the estimated loss rate due to surface heating is more sensitive to the KBO density than is loss due to upper atmosphere heating. Finally, for Charon orbiting Pluto, we reduced the gravitational binding by a factor of 0.91 assuming escape occurs if molecules reach its Hill sphere.

For a number of the KBOs the SJ approximation is seen in Table 2 to hugely overestimate the loss of N_2 due to solar heating of the surface. With the exception of Sedna, which has an extremely thin atmosphere in its present orbit, it is seen that the upper atmospheric heating dominates the net mass loss for all KBOs studied even for a thick early N_2 atmosphere on Charon. As in SB we estimate the net loss of N_2 assuming that the trajectory and properties are unchanged for most of the lifetime of the KBO. If we assume each KBO is in its present orbit for $\tau \sim 4.5$ Gyr (1.4×10^{17} s) and the initial mass fraction of N_2 is f_{N2}, the fractional loss, f_{loss}, of the initial inventory of N_2 is

$$f_{loss} = [\langle dM/dt\rangle \tau]/\left[f_{N_2} M_{KBO}\right]. \quad (6)$$

Using Equation (6) implies that all of the N_2 eventually has access to the surface by diffusion from the interior, which may be unlikely. Values for f_{loss} are given in Table 2 using the mass fraction of nitrogen suggested in SB, $f_{N2} = 0.0074$. The present estimates indicate even at Charon, which does not appear to have retained a primordial N_2 atmosphere, the escape rate is dominated by upper atmospheric heating with the approximate loss time given in brackets.

Before discussing the relevance of the results in Table 2, we note that since EUV/UV heating of the upper atmosphere dominates, the higher fluxes in the early solar system can significantly decrease the time for a KBO to lose its primordial N_2. Ribas et al. (2005) showed that the EUV/UV radiation could be roughly scaled by time, t, as $F_0\,(4.56\,\mathrm{Gyr}/t)^y$ with F_0 the present flux. For Lyα they estimated $y \sim 0.72$ and for the radiation in the 92–110 nm, range $y \sim 0.85$. For the EUV in the 80–100 nm range absorbed by N_2, they estimated $y \sim 1.27$. If we assume the KBO's orbit, absorption efficiencies and heating efficiencies do not change significantly, as assumed in estimating f_{loss}, then the effective flux averaged from ~0.1 Gyr to the present is enhanced by about a factor of 2.3 for the Lyα absorbed by CH_4 and a factor of ~6.7 for the EUV contribution to the energy absorbed by N_2. Assuming a KBO is in its orbit for nearly the lifetime of the solar system the resulting heat flux at 30 AU is about three times that typically used for solar medium at 30 AU, enhancing the loss rate by a factor of ~3. In which case Pluto would have retained only ~60% of its initial N_2 and Makemake and Quaoar would likely have lost all of their N_2. Of course, these bodies were probably *not* in their present orbits for the lifetime of the solar system nor would the albedo remain fixed during the evolution of the atmospheres, points that will be examined in the future. However, larger loss rates than those in Table 2 are likely.

SUMMARY

Guided by recent simulations, we have presented new estimates of the loss of the primordial nitrogen from a number of large KBOs accounting for escape of N_2 driven by surface

Table 2
Orbital-averaged Mass Loss Rates (kg s^{-1})

KBO	$\langle dM/dt\rangle_{SJ}$	$\langle dM/dt\rangle_{S}$	$\langle dM/dt\rangle_{U}$	$\langle dM/dt\rangle$	f_{loss}	Δr_{KBO}(km)
Eris	1.80×10^{-28}	4.6×10^{-28}	30.	16.	0.018	0.13
Triton	1.1×10^{-24}	9.7×10^{-24}	130.	130.	0.11	1.1
Pluto	1.4×10^{-16}	1.2×10^{-15}	83.[a]	83.	0.11	0.7
Makemake	12.−0.013	4.1−0.078	81.−62.	81.−62	0.58–0.34	1.2–0.7
Quaoar	1.4×10^{3}	11.	64.	64.	0.88	2.4
2007OR10	$5.2-0.043 \times 10^{3}$	3.1−1.4	49.−38.	29.−22.	0.31−0.18	0.77−0.55
Charon	1.8×10^{5}	17.	110.	110	All {3.5 Gyr}	2.4
Sedna	$(8.4-0.1) \times 10^{-3}$	$(16.-2.6) \times 10^{-3}$	15.−11.	$(16-2.6) \times 10^{-3}$	0.018	0.13

Notes. Orbital-averaged loss rates for a primordial N_2 atmosphere containing a small fraction of CH_4: calculated using parameters from Table 1 but with $A = 0.67$ and $\varepsilon = 0.8$. Results for Charon are corrected for escape due to its Hill sphere and results for Makemake, 2007OR10, and Sedna are given for low and high densities in Table 1. $\langle dM/dt\rangle_{SJ}$: orbital average SJ loss rate using Equation (1*b*) as in SB; $\langle dM/dt\rangle_{S}$: orbital averaged loss rate due to surface heating using Equation (2*b*); $\langle dM/dt\rangle_{U}$: orbital averaged loss induced by upper atmosphere heating using Equation (4) *not* requiring $N_0 > N_c$; $\langle dM/dt\rangle$: net orbital-averaged loss rate using the larger of $\langle dM/dt\rangle_{S}$ and $\langle dM/dt\rangle_{U}$ and requiring that $N_0 > N_c$; f_{loss}: fraction lost of N_2 in Equation (6) for $\tau = 4.5$ Gyr using the initial mass fraction of N_2 from SB, $f_{N_2} = 0.0074$; {} time to lose the primordial N_2 if it can all eventually diffuse to the surface; Δr_{KBO}: rough radial change assuming compaction during loss of N_2, $\Delta r = \{\tau \langle dM/dt\rangle/[4\pi\ \rho_{N2} R_{KBO}^2]\}$ with $\rho_{N2} = 1.0$ gm cm^{-3}.
[a] Used density in Erwin et al. (2013) and not more recent value in Table 1 a 10% effect.

and atmospheric heating. The estimates in Table 2 are based on the assumption that the volatile fraction of N_2 assumed in SB is roughly correct, that all of the N_2 can eventually diffuse to the surface from which it can sublime into the atmosphere, that the presence of CH_4 in the early, predominantly N_2, atmospheres affects only the heating rate, the KBO orbital parameters did not change for ∼4.5 Gyr, that other loss processes, such as large impacts, are ignored, and that $A \sim 0.67$ and $\varepsilon = 0.8$ during the period the KBO retains a significant N_2 atmosphere and a surface frost. Allowing for these rather drastic assumptions, the rates estimated in Table 2 show that the loss due to heating of the upper atmosphere *dominates* the escape of nitrogen for *all of* the objects discussed, except possibly Sedna.

With these improved estimates of the loss rate, we re-examine the relationship between atmospheric retention and observed KBO properties discussed by Schaller & Brown (2007). It is seen in Table 2 that even the largest KBO's can have significant mass loss rates, as much as a kilometer of material possibly affecting the morphology of their surface features. However, they still retain a significant fraction of their initial N_2 inventory, consistent with observations. Therefore, precipitation of a bright N_2 frost appears to correlate with their higher bond albedos as pointed out in SB. Even if we account for the enhancement in the EUV/UV flux in the early solar system, Eris, Triton and Pluto would retain much of their initial N_2 inventory. On the other hand, if we include the enhancement in the UV in the early solar system, Makemake might have been expected to lose its full component of primordial N_2 contrary to what is suggested by the observation of its relatively bright surface ($A \sim 0.62$).

The very low albedos ($A < 0.1$) on Quaoar and 2007OR10 have been attributed to radiation-induced production of hydrocarbons that dominate the surface when the primordial N_2 is lost. Of course, as at Titan, the UV photolysis of CH_4, which heats the upper atmosphere, also produces hydrocarbons and a precipitate *while* the KBO retains an N_2 atmosphere. By scaling to results for Titan (e.g., Strobel 1974; Atreya et al. 2006), the mass loss rate due to photolysis and precipitation of CH_4 products is smaller than $\langle dM/dt\rangle_{U}$ in Table 2, but could affect the surface reflectance. However, as long as the N_2 component is robust, we presume, as did SB, that condensation will cover much of the precipitate with a frost. After most of the N_2 escapes there might be a residual CH_4 atmosphere with a surface that becomes increasingly dark in the visible due to the precipitates, or to direct irradiation carbon species on the surface (e.g., Johnson 1989). Although this picture is likely correct, for these two bodies the complete loss of the primordial N_2 inventory is not easily explained by the results in Table 2 if the initial inventories are correct and no nitrogen is sequestered below the surface. Allowing for a contribution from the enhanced UV in the early solar system, this picture *would be* consistent with the results for Quaoar, although observations suggest the possible presence of some N_2. However, for 2007OR10, which has a very small albedo ($A \sim 0.06$), loss of its full N_2 inventory is problematic even when increasing f_{loss} by a factor of three. That is, in the model described here complete loss would require the most extreme assumptions: the lowest density in Table 1, a low albedo as in Figure 4, and being in its present orbit for nearly the lifetime of the solar system experiencing the enhanced UV/EUV flux. Although this is all possible, more detailed modeling is required for 2007OR10 to determine if some other loss process such as a large impact might have occurred, whether N_2 is sequestered below its surface, or whether it had a different initial inventory. Because the ratio $\langle dM/dt\rangle_{S}/\langle dM/dt\rangle_{U}$ in Table 2 is largest for this intermediate-sized body, synergy between the surface and upper atmospheric heating could be important, an aspect we will be examining.

Unlike Quaoar, 2007OR10 is in a very eccentric orbit. During the period of time that 2007OR10 retains most of its nitrogen component and a bright surface, the N_2 atmosphere would collapse at ∼70 AU in our model. Beyond this point the surface becomes directly exposed to charged particle radiation, especially as it approaches the terminator shock at 80 AU and the heliopause at ∼100 AU. This exposure could gradually reduce its albedo, enhancing the loss rate as indicated in Figure 4. In this regard, it is also interesting to compare 2007OR10 to Eris, which has a similarly eccentric orbit and, in its present location (∼100 AU), has an albedo somewhat smaller than the other large objects. As 2007OR10 and Eris approach aphelion, they both cross the $N_0 > N_c$ solid curve in Figure 3 in which case surface heating can dominate. That escape rate is, however, strongly affected by their large mass difference and, as seen in Figure 3, any darkening increases

the period of time which loss due to upper atmospheric heating dominates. Whereas the contributions in Table 2 to escape from Eris are small, this is not the case for 2007OR10. Therefore, the evolution of the surface reflectance needs to be treated along with atmospheric escape, work that is now in progress.

Based on the albedos and loss rates, there are two outliers, Charon and Sedna. In its present orbit, Sedna's atmosphere is always thin and it spends much of its time outside the heliosphere. That is, although Sedna retains its primordial N_2, it is primarily frozen N_2 on the surface, along with CH_4, with only a very tenuous atmosphere. Therefore, the surface reflectance is affected by the long-term irradiation of a mixed surface ice. The results in Table 2 also indicate that, if the primordial volatiles eventually all diffuse to the surface, Charon would have lost its initial N_2 inventory $\sim$1 Gyr ago, as is likely also the case for its CH_4 inventory. Charon's surface is, therefore, dominated by water ice, possibly having regions with trapped nitrogen-containing molecules (Cook et al. 2007; Neveu et al. 2015). Such molecules could be from residual primordial nitrogen or nitrogen delivered by comets (Stern et al. 2015). However, Pluto's escaping atmosphere continuously delivers N_2, which forms a thin atmosphere over the warmest regions but accumulates as a frozen layer in the cold regions until exposure to the Sun (Tucker et al. 2015) a concept that will be tested during the New Horizon encounter.

We have shown here that the connection between the surface properties and atmospheric escape may be more subtle and interesting than suggested earlier. As knowledge of the physical properties of the KBOs, their orbital history and the initial volatile inventory improve the methods for estimating atmospheric loss given here can provide guidance when describing the volatile history. However, much more detailed simulations are needed on individual KBOs, taking into account surface and upper atmosphere heating as well as the fate of CH_4. Now that it is clear that the upper atmospheric heating is critical, such simulations are in progress.

The work at Virginia was supported by grants from NASA's Outer Planet Research and Planetary Atmospheres Programs.

REFERENCES

Abernathy, M. R., Tegler, S. C. W. M., Grundy, W. M., et al. 2009, Icar, 199, 520
Atreya, S. K., Adams, E. Y., Niemann, H. B., et al. 2006, P&SS, 54, 1177
Barucci, M. A., Dalle Ore, C. M., Alvarez-Candal, A., et al. 2010, AJ, 140, 2095
Braga-Ribas, F. 2013, PhD thesis, Ministério da Ciencia, Tecnologia e Inovacão Observatório Nacional
Braga-Ribas, F., Sicardy, B., Ortiz, J. L., et al. 2013, ApJ, 773, 26
Brown, M. E., Barkume, K. M., Blake, G. A., et al. 2007a, ApJ, 133, 284
Brown, M. E., Barkume, K. M., Ragozzine, D., & Schaller, E. L. 2007b, Natur, 446, 294
Brown, M. E., Burgasser, A. J., & Fraser, W. C. 2011, ApJL, 738, L26
Brown, M. E. 2012, AREPS, 40, 467
Brozović, M., Showalter, M. R., Jacobson, R. A., & Buie, M. W. 2015, Icarus, 246, 317
Buie, M. W., Grundy, W. M., Young, E. F., Young, L. A., & Stern, S. A. 2006, AJ, 132, 290
Cook, J. C., Desch, S. J., Roush, T. L., Trujillo, C. A., & Geballe, T. R. 2007, ApJ, 663, 1406
Dalle Ore, C. M., Barucci, M. A., Emery, J. P., et al. 2009, A&A, 501, 349
DeMeo, F. E., Dumas, C., de Bergh, C., et al. 2010, Icar, 208, 412
Elliot, J. L., Dunham, E. W., Bosh, A. S., et al. 1989, Icar, 77, 148
Elliot, J. L., & Young, L. A. 1992, AJ, 103, 991
Emery, J. P., Dalle Ore, C. M., Cruikshank, D. P., et al. 2007, A&A, 466, 395
Erwin, J., Tucker, O. J., & Johnson, R. E. 2013, Icar, 226, 375
Fornasier, S., Lellouch, E., & Müller, T. 2013, A&A, 555, A15
Gladstone, G. R. 1998, Lyman-α photolysis in the Primitive Solar Nebula, Final Report for NASA Grant NAG5-4290
Grundy, W. M., Olkin, C. B., Young, L. A., & Holler, B. J. 2014, Icar, 235, 220
Grundy, W. M., Young, L. A., Stansberry, J. A., et al. 2010, Icar, 205, 594
Gruzinov, A. 2011, arXiv: 1101.1103v1
Gulbis, A. A. S., Elliot, J. L., & Person, M. J. 2006, Natur, 439, 48
Holler, B. J., Young, L. A., Grundy, W. M., Olkin, C. B., & Cook, J. C. 2014, Icar, 243, 104
Johnson, R. E. 1989, GeoRL, 16, 1233
Johnson, R. E., Volkov, A. N., & Erwin, J. T. 2013a, ApJL, 768, L4
Johnson, R. E., Volkov, A. N., & Erwin, J. T. 2013b, ApJL, 779, L30
Krasnopolsky, V. A. 1999, JGR, 104, 5955
Krasnopolsky, V. A., & Cruikshank, D. P. 1999, JGR, 104, 21979
Lammer, H., Odert, P., Leitzinger, M., et al. 2009, A&A, 506, 399
Lellouch, E., de Bergh, C., Sicardy, B., Ferron, S., & Käufl, H.-U. 2010, A&A, 512, L8
Lellouch, E., Sicardy, B., de Bergh, C., et al. 2009, A&A, 495, L17
Lellouch, E., Stansberry, J., Emery, J., Grundy, W., & Cruikshank, D. P. 2011, Icar, 214, 701
Levi, A., & Podolak, M. 2009, Icar, 202, 681 (LP)
Lim, T. L., Stansberry, J., Müller, T. G., et al. 2010, A&A, 518, L148
McKinnon, W. B., Lunine, J. I., & Banfield, D. 1995, Neptune and Triton, (Tucson, AZ: Univ. Arizona Press), 807
Neveu, M., Desch, S. J., Shock, E. L., & Glein, C. R. 2015, Icar, 246, 48
Ortiz, J. L., Thirouin, A., Campo Bagatin, A., et al. 2012, Natur, 491, 566
Pál, A., Kiss, C., Müller, T. G., et al. 2012, A&A, 541, L6
Person, M. J., Elliot, J. L., Gulbis, A. A. S., et al. 2006, AJ, 132, 1575
Quémerais, E., Sandel, W. R., Izmodenov, V. V., & Gladstone, G. R. 2013, in Thirty Years of Interplanetary Background Data: A Global View. 2013, ISSI Sci. Report Ser. 13, ed. E. Quémerais et al. (New York: Springer)
Ribas, I., Guinan, E. F., Güdel, M., & Audard, M. 2005, ApJ, 622, 680
Santos-Sanz, P., Lellouch, E., Fornasier, S., et al. 2012, A&A, 541, A92
Schaller, E. L., & Brown, M. E. 2007, ApJ, 670, 49 (SB)
Sicardy, B., Ortiz, J. L., Assafin, M., et al. 2011, Natur, 478, 493
Stansberry, J., Grundy, W. W., Brown, M., et al. 2008, The Solar System Beyond Neptune, ed. M. A. Barruci, (Tucson, AZ: Univ. Arizona Press)
Stansberry, J. A., Lunine, J. I., Porco, C. C., & McEwen, A. S. 1990, GeoRL, 17, 1773
Stern, S. A., Gladstone, R., Zangari, A., Goldstein, D., & Fleming, T. 2015, Icar, submitted
Strazzulla, G., Cooper, J. F., & Johnson, R. E. 2003, CRPhy, 1, 791
Strobel, D. F. 1974, Icar, 21, 466
Strobel, D. F., Zhu, X., Summers, M. E., & Stevens, M. H. 1996, Icar, 120, 266
Tegler, S. C., Grundy, W. M., Olkin, C. B., et al. 2012, ApJ, 751, 76
Tegler, S. C., Grundy, W. M., Vilas, F., et al. 2008, Icar, 195, 844
Thomas, P. C. 2000, Icar, 148, 587
Tucker, O. J., Erwin, J. T., Deighan, J. I., Volkov, A. N., & Johnson, R. E. 2012, Icar, 217, 408
Tucker, O. J., & Johnson, R. E. 2009, P&SS, 57, 1889
Tucker, O. J., Johnson, R. E., & Young, L. A. 2015, Icar, 246, 291
Volkov, A. N. 2015, ApJL, submitted
Volkov, A. N., & Johnson, R. E. 2013, ApJ, 765, 90
Volkov, A. N., Johnson, R. E., Tucker, O. J., & Erwin, J. T. 2011a, ApJL, 729, L24
Volkov, A. N., Tucker, O. J., Erwin, J. T., & Johnson, R. E. 2011b, PhFl, 23, 066601
Yelle, R. V. 2004, Icar, 170, 167
Yelle, R. V., Lunine, J. I., Pollack, J. B., & Brown, R. H. 1995, in Neptune and Triton (Tucson, AZ: Univ. Arizona Press), 1031
Young, L. A. 2012, Icar, 221, 80
Young, L. A. 2013, BAAS, 45, 507.02
Zhu, X., Strobel, D. F., & Erwin, J. T. 2014, Icar, 228, 301